VILNIUS UNIVERSITY

CENTER FOR PHYSICAL SCIENCE AND TECHNOLOGY

VYTAUTAS RUMBAUSKAS

PECULIARITIES OF CARRIER SCATTERING AND THERMAL EMISSION IN LARGE FLUENCE IRRADIATED SILICON

Summary of doctoral dissertation

Physical sciences, Physic (02P)

Vilnius, 2016

Doctoral dissertation was prepared during period of 2011-2016 years at Vilnius University Faculty of Physics

Supervisor – Prof. Dr. Sc. Juozas Vidmantis Vaitkus (Vilnius University, Physical Sciences, Physic – 02P)

Thesis defended at the united Vilnius University and CPST Physics research council:

Chairman – Prof. Dr. Vincas Tamošiūnas (Vilnius University, Physical science, Physic – 02P).

Members:
Prof. Dr. Sc. Artūrs Medvids (Ryga Technical University, Physical science, Physic – 02P);
Doc. Dr. Artūras Plukis (Vilnius University, Physical science, Physic – 02P);
Doc. Dr. Tomas Šalkus (Vilnius University, Science of technology, Material engineering – 08T);
Doc. Dr. Bonifacas Vengalis (Center of Physical Science and Technology, Science of technology, Material engineering – 08T).

The dissertation will be defended on 19th of September in 201, 4 PM in auditorium Nr. B336 in National Center of Physical Science and Technology, Saulėtekio av. 3, LT-10257, Vilnius, Lithuania.

Summary of dissertation sent on 17th of August in 2016.

The dissertation is available at Vilnius University, Center of Physical science and technology libraries and on internet: *www.vu.lt/lt/naujienos/ivikiu-kalendorius*

VILNIAUS UNIVERSITETAS

FIZINIŲ IR TECHNOLOGIJOS MOKSLŲ CENTRAS

VYTAUTAS RUMBAUSKAS

KRŪVININKŲ SKLAIDOS IR TERMINĖS AKTYVACIJOS YPATUMAI DIDELIAIS ĮTĖKIAIS APŠVITINTAME SILICYJE

Daktaro disertacijos santrauka

Fiziniai mokslai, fizika (02 P)

Vilnius, 2016 metai

Disertacija rengta 2011-2016 metais Vilniaus universitete Fizikos fakultete.

Mokslinis vadovas – prof. habil. dr. Juozas Vidmantis Vaitkus (Vilniaus universitetas, fiziniai mokslai, fizika – 02P).

Disertacija ginama jungtinėje Vilniaus universiteto ir FTMC Fizikos mokslo krypties taryboje:

Komisijos pirmininkas – prof. dr. Vincas Tamošiūnas (Vilniaus universitetas, fiziniai mokslai, fizika – 02P).

Nariai:
Prof. habil. dr. Artūrs Medvids (Rygos technikos universitetas, fiziniai mokslai, fizika – 02P);
Doc. dr. Artūras Plūkis (Vilniaus universitetas, fiziniai mokslai, fizika – 02P);
Doc. dr. Tomas Šalkus (Vilniaus universitetas, technologijos mokslai, medžiagų inžinerija – 08T);
Doc. dr. Bonifacas Vengalis (Fizinių ir technologijų mokslų centras, technologijos mokslai, medžiagų inžinerija – 08T).

Disertacija bus ginama 2016 m. rugsėjo 19 d. 16^{00} val. B336 auditorijoje Nacionaliniame fizinių ir technologijų mokslų centre, Saulėtekio al. 3, LT-10257, Vilnius, Lietuva.

Disertacijos santrauka išsiuntinėta 2016 m. rugpjūčio 17 d.

Su disertacija galima susipažinti Vilniaus universiteto, Fizinių ir technologijos mokslų centro bibliotekose ir VU interneto svetainėje adresu: *www.vu.lt/lt/naujienos/ivikiu-kalendorius*

List of abbreviations used in the text

CERN   − (*Conseil Européen pour la Recherche Nucléaire*) European Organization for Nuclear Research.

CZ   − Czochralski method of crystal growth

DFT   − Density Functional Theory

DOFZ   − Diffusion Oxygenated Float Zone

DLTS   − Deep Level Transient Spectroscopy

EPR   − Electron Paramagnetic Resonance spectroscopy

FTIR   − Fourier Transform Infrared spectroscopy

FZ   − Float Zone method of crystal growth

LHC   − Large Hadron Collider

MCZ   − Magnetic field applied Czochralski method of crystal growth

MW-PC   − Microwave Probed Photoconductivity

TDTL   − Temperature Dependent Trapping Lifetime

TSC   − Thermally Simulated Current

PL   − Photo Luminescence

Introduction

Research problem. Detection of ionizing radiations is one of the important trends in technology of modern applications of the radiological diagnostics and therapy in medicine as well as in fundamental research of elementary particles. As an example of such applications, the positron based tomography is the increasingly growing technique in imaging of the human body organs over radiological diagnostics. Another illustration of the demand of radiation tolerant detectors can be found in the experiments of high energy physics performed on Large Hadron Collider in CERN, where the amazing discoveries have been made in Standard Model theory by justifying the existence of Higgs field and boson. Silicon based particle trackers and other type sensors are the most spread detectors in the nowadays electronics exploited in different areas of radiation monitoring. Nevertheless, a big challenge appears when silicon detectors of the standard technology should withstand particle flows of $>10^{35}$ cm^{-2}s^{-1} and fluences of $>10^{16}$ cm^{-2} in CERN applications. Approaching of these limits leads to a dramatic increase of sensor leakage currents to the unacceptable reduction of charge collection efficiency. Enhancement of leakage currents is mainly related with increased carrier trapping and thermal emission from centres introduced by radiations. Charge collection efficiency is determined by carrier transport parameters in the heavily irradiated materials. Thus, research of carrier scattering and thermal emission characteristics in heavily irradiated Si materials is inevitable in order to predict the operational characteristics of particle sensors made of Si and to invent the methods of defect engineering as well as of device architecture to enhance radiation tolerance of Si based sensors.

The main defect engineering techniques are based on selection of particular dopant species (such as introduction of oxygen impurities) and variation of doping level of Si material. These technological means allows suppressing of the harmful defect reactions and a reduction of the expedient doping level, to keep an operational device. Nevertheless, the radiation introduced point-like and extended defects as well as dopants act as the efficient carrier scattering centres thereby affecting functional parameters of detectors. The extended radiation defects determine appearance of the local and stochastically distributed space charge regions within active layers of sensors by reducing homogeneity of material. On the other hand, these complicated defects are a reason for the more intricate carrier trapping and emission processes. The device design methods, such as usage of the internal gain regimes based on the avalanche processes under impact ionization, also needs knowledge concerning peculiarities of carrier scattering and trapping/emission characteristics in heavily irradiated Si material.

Thereby, this research was addressed to proximate study of the carrier scattering parameters by using the most suitable and direct methods of Hall effect and magnetoresistance measurements. Synchronously, the interplay among the processes of carrier injection, trapping as well as thermal emission and carrier scattering within a system of radiation defect-rich had been anticipated to research by employing spectroscopy methods such as DLTS and photo-ionization. The contact and contact-less techniques have been combined to clarify the role of contacts and large fluence irradiated bulk Si material, made using different growth and doping technologies.

Objectives of research. This work was addressed to study of carrier scattering, injection and thermal emission processes in silicon materials fabricated using different techniques in order to make models of dominant mechanisms for these processes and to establish the most relevant methods and reliable regimes for assessment of the parameters of the carrier scattering and thermal emission for prediction of material radiation hardness.

The tasks were concentrated on:

- search of the most reliable methods for measurements of carrier transport parameters under conditions when radiation defect ascribed space charge regions may considerably reduce Hall voltage in evaluation of carrier mobility;
- spectroscopy of carrier injection processes by photo-ionisation and thermal emission and of interplay of these processes in radiation defect-rich silicon materials;
- spectroscopy of radiation induced defects by combining several techniques for the comprehensive and reliable characterization of Si materials by covering a wide range of the radiation induced trap and effective doping densities;
- design of models of the dominant mechanisms of carrier thermal emission and scattering phenomena in Si over a wide range of temperatures and irradiation fluences
- investigation of radiation defect transforms under heat treatment procedures of the heavily irradiated Si.

Relevance and scientific novelty. Despite of big progress in design and production of silicon particle detectors, there still exist the specific tasks in passivation of defects and suppression of their interplay, in evaluation of barriers and space charge regions in radiation damaged materials for production of the radiation hard detectors. In this research, it has been demonstrated that synchronous measurements of Hall and magnetoresistance mobility can be a reliable tool for monitoring of irradiation caused variations of carrier scattering mechanism. It has been revealed that the ratio of magnetoresistance and Hall mobilities retains value of 1.15±0.25 over wide range of fluences. There it was unveiled that the main reason for reduction of Hall voltage in heavily irradiated Si is formation of the intersecting space charge regions due to extended radiation induced cluster type defects those screen formation of Hall field. The model of radiation cluster has been proposed where specific of carrier scattering and tunnelling through the cluster surrounding barrier are incorporated. It has been evaluated the threshold energy for creation of Frenkel pair type radiation defect in p-Si material is 2 eV, when space charge regions coalesce at radiation fluences of $\geq 8 \times 10^{16}$ cm^{-2} and saturate, while energy of Frenkel pair creation in n-Si varies in the range from 12 eV to 2 eV and depends on irradiation fluence. The role of the electron-phonon interaction has been evaluated ascribed to radiation defects. The hysteresis type spectral and temperature dependent characteristics of the photo-ionization response have been clarified in heavily irradiated Si detectors where cluster type defects with strong electron-phonon interaction are inherent. The combined technique based on optical-injection current-probed deep level transient spectroscopy and temperature scanned trapping lifetime spectroscopy has been approved to trace reactions and transforms of defects in Si introduced by large fluence irradiations.

Practical importance. Several advanced techniques and novel methodologies for characterization of large fluence irradiated silicon materials have been proposed and approved.

The dominant species of radiation defects in heavily irradiated Si have been clarified. The anneal temperatures of different type defects and their transform paths were either verified or revealed. This paves grounds for advanced technologies of defect engineering in hardening of the radiation tolerance of modern Si materials and in design of operation regimes of the new generation sensors.

Statements in defence. The main statements in defence of this thesis are as follows:

1. The inherent reduction of Hall voltage in large fluence irradiated Si is caused by enhanced density of space charge regions and their. Therefore, the synchronous measurements of Hall and magnetoresistance mobilities with their ratio at 1.15 are recommended for the comprehensive and reliable analysis of carrier scattering mechanisms in heavily irradiated Si.

2. The threshold energy for creation of Frenkel pair type radiation defect in p-Si material is 2 eV, while, the energy of Frenkel pair creation in n-Si varies in the range from 12 eV to 2 eV and this energy depends on irradiation fluence.

3. The cluster type radiation defects are created under large fluence neutron irradiations of Si those act as the dominant carrier scattering and thermal emission centres, for which strong electron-phonon interaction and phonon assisted tunnelling through cluster barriers is inherent. The tunnelling efficiency depends on a width of the cluster barrier determined by spreading of the space charge region surrounding the cluster core.

4. The contact-less technique of temperature scanned carrier trapping lifetime spectroscopy is the most relevant tool for analysis of interaction of several radiation defects acting as carrier recombination and thermal emission centres, in heavily irradiated Si material.

Author's contribution. During this study, author has performed measurements on Hall effect and magnetoresistance, on photo-ionisation and DLTS spectroscopy. Author performed simulations and fitting of the experimental characteristics of carrier mobility and material conductivity, and various spectra, as well. The main results of dissertation author presented within a set of international ("International Workshop of Radiation Imaging Detectors", "Radiation Interaction with Material and Its Use in Technologies","Workshop on Radiation hard semiconductor devices for very high luminosity colliders") and national ("Lithuanian national physics conference" LNFK40 in 2013) conferences. Author has prepared several drafts of article manuscripts.

Several experimental studies were performed in collaboration with PHD student D. Meskauskaite, Dr. T. Ceponis, and Dr. Sc. E. Gaubas. A few of publications were prepared in collaboration with Dr. A. Mekys, Dr. E. Zasinas. Writing of the final versions of manuscripts were made by supervisor Prof., Dr. Sc. J. Vaitkus. Several investigations and publications were performed under supervision of Dr. Sc. E. Gaubas.

Publications. The main results of this study are published within 4 scientific articles [S1-S4] and the research results have been approved within 13 oral and poster presentations.

Content of dissertation

In the **introduction chapter**, the research item, objectives and tasks of this research, relevance and scientific novelty of the performed investigations, practical importance of the findings within this dissertation work, statements on defence are briefly discussed. Also, author's contribution is there defined and a list of the main published articles as well as conference presentations is attached.

The **I-st chapter** is devoted to a review of literature on radiation defects, on their performance within operational characteristics of particle detectors made of silicon, manifestation of the radiation defects within galvano-magnetic phenomena and characteristics, to motivate the most important issues and trends of research. The main techniques of radiation defect spectroscopy are also surveyed in this chapter.

Within **chapter II**, the investigated materials and employed characterization techniques are described in the second chapter.

The geometry and electrode system of Si samples exploited in the Hall effect and magnetoresistance measurements is there described. Technology of the Schottky diode and ohmic contact formation is sketched. The routine characteristics of I-V and C-V, used in primary evaluations of contact quality and estimations of material conductivity, are there presented and briefly discussed. The regimes and parameters of irradiations and anneals are denoted. A list of the examined Si materials, fabricated by different technologies, as MCZ, CZ, FZ, DOFZ and invoked into these investigations, is presented.

Techniques and instrumentation for measurements of the Hall effect, of magnetoresistance and material conductivity are presented in the third chapter. The scattering factors ascribed to Hall (μ_H) and magnetoresistance (μ_{GMR}) mobilities are discussed, where these mobilities are related as

$$\mu_{GMR} = \xi \mu_H \qquad (2.1)$$

with ξ standing for the scattering factor which is ascribed to magnetoresistance and expressed through inherent scattering times τ as

$$\xi = \left(\langle \tau^3 \rangle \langle \tau \rangle / \langle \tau^2 \rangle^2 \right). \qquad (2.2)$$

The methodical aspects within examination of the magnetoresistance dependencies on the applied magnetic induction B and on geometrical dimensions as well as factors of samples (illustrated in Fig. 2.1) are discussed.

The main assumptions of $\rho_B \approx \rho_0$, $\mu_{GMR} \approx \mu_H$ as well as $\mu_H \approx \mu_p$ and the fundamental relations among Hall (μ_H), magnetoresistance (μ_{GMR}) and drift (μ_p) mobilities are there defined. To get the proper approximations for evaluation of experimental parameters, these relations are expressed as:

$$\frac{R_B}{R_0} = \frac{\rho_B}{\rho_0} \left[1 + \left(\mu_{GMR} B \right)^2 \left(1 - 0{,}54 L/W \right) \right]; \qquad (2.3)$$

$$\mu_p \approx \frac{1}{B}\sqrt{\frac{R_B}{R_0} - 1} \; ; \qquad (2.4)$$

and

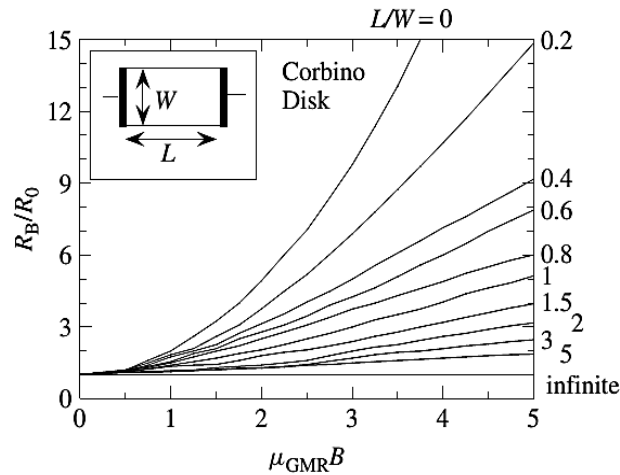$$\mu = \frac{1}{B}\left(\frac{I_0}{I_B} - 1\right)^{1/2} . \qquad (2.5)$$

Fig. 2.1. Magnetoresistance as a function of magnetic induction B for the square-shaped samples with different ratios between sample length L and its width W.

Instrumentation (sketched in Fig. 2.2), exploited in measurements of Hall effect, of magnetoresistance and of material conductivity contains precise electrometers and voltage sources as well as Hall sensors to reliably control the measured variables. There, the devices for temperature and vacuum maintaining and control are installed. All the procedures of measurements, data sampling and primary analysis are controlled by a personal computer.
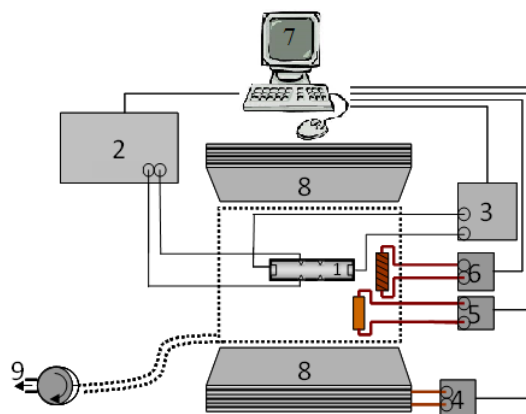
Fig. 2.2. Sketch of the instrument for examination of the galvano-magnetic characteristics: 1-sample; 2-electrometer; 3-voltge source; 4-magnet current source; 5-thermo-couple; 6-heater; 7-personal computer; 8-magnet; 9-vacuum-pump.

The technique and instrumentation exploited for spectroscopy of the photo-ionisation is also described in Chapter II. Photon capture cross-section $\sigma_{h\nu}$ is extracted by analysis of the photo-current spectral dependence. In the case of weak electron-phonon interaction, the spectral variation of the cross-section of the photon-electron interaction is commonly described by Lucovsky model [1]:

$$\sigma_{h\nu} \sim \Delta E_M^{0.5}(h\nu - \Delta E_M)^{1.5}/(h\nu)^3 . \qquad (2.6)$$

In the case of strong electron–phonon interaction, this dependence is modified using torsion with Gaussian function where photo-activation energy ΔE_M is a variable. Also, an assumption of spread distribution of levels with ΔE_M is there employed.
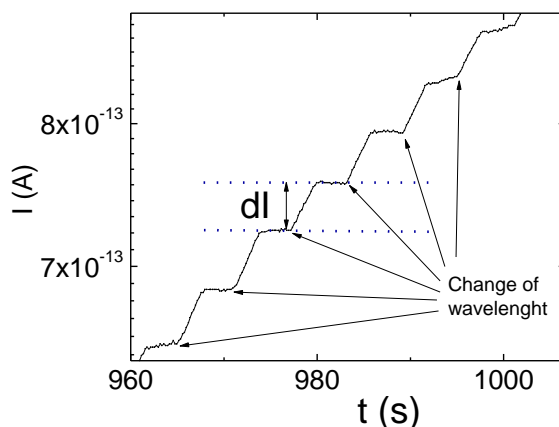
Fig. 2.3. Transients of photo-current under the change of photon energy. The proper delay time after a sudden change of photon energy is chosen to reach the stabilization of photo-current, which saturated value is recorded to get the spectral characteristic of photo-ionization.
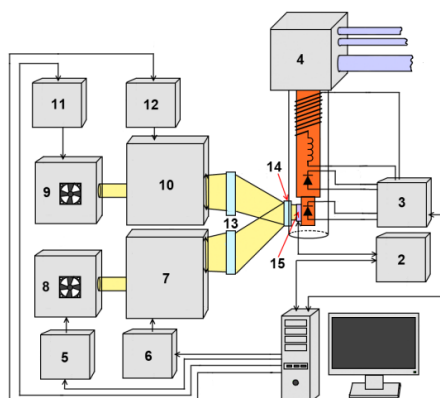

Fig. 2.4. Sketch of the experimental arrangement for spectroscopy of photo-ionization: 1-personal computer; 2-universal source meter HP4140B; 3-temperature controller Scientific Instruments 9700; 4-closed-cycle helium cryostat; 5- current source CPX400DP; 6-step-motor controller; 7-prism monochromator DMR-4; 8-light source; 9- light source (halogen lamp or Nernst stick); 10-monochromator Bentham-TMc300; 11- current source Bentham-608; 12-step-motor controller Bentham-PMC-MAC; 13-focusing optics; 14-cryostat window; 15-sample.

In the case of cluster type radiation defects, the photon-electron interaction is complicated due to existence of space charge barriers those are able to separate excess electrons and holes. This leads to phenomena of charge accumulation and of hysteresis in spectral variations of the photo-current signals. In this case, the measurement procedure, using delay for current stabilization, and analysis approach (with assumption of the step-like (shown in Fig. 2.3) increase of photon energy within spectral changes of the photo-current) have been proposed. The energy is there enhanced by a small step, and the change of the stabilized current value is measured.

A sketch of the experimental arrangement exploited in photo-ionization spectroscopy measurements is presented in Fig.2.4. The measurement procedures and primary analysis of the experimental data are controlled by a personal computer.

The thermal emission characteristics have been examined using the deep level transient spectroscopy (DLTS) technique. The standard capacitance C-DLTS technique is appropriate, when capacitance variations due to excess carriers emitted from traps into continuum states are rather small. Then, DLTS signal is proportional to the ratio of trap concentration (N_T) to that of the effective doping (N_{Def}). The time varied barrier capacitance change determined by the majority carrier emission from deep levels can be expressed as:

$$\frac{\Delta C(t)}{C} = \begin{cases} -\frac{1}{2}\frac{N_T}{N_{Def}}e^{-e_n t}, & e_n >> e_p \\ 0, & e_n << e_p \end{cases} .$$ (2.7)

Here, C is the barrier capacitance value under reverse bias for a fixed voltage, $\Delta C(t)$ is the capacitance change due to the emission of carriers from the definite type deep level, $e_{n,p}$ is the emission rate for electrons and holes, respectively. C-DLTS method is appropriate when the N_T concentration is less than 10% of the shallow dopant (N_{Def}) concentration [2, 3]. Therefore current deep level transient spectroscopy (I-DLTS) method is preferable for the defect-rich irradiated samples [3-5]. The I-DLTS signal does not depend directly on N_{Def} value, and there is no limitation for the ratio of N_T/N_{Def} [6]. The total current density is then expressed by relation:

$$J(t) = -\frac{1}{2}qx_d N_T \frac{e_n}{e_n + e_p}\left[2e_p + \left(e_n - e_p\right)e^{-(e_n+e_p)t}\right] = J_L + \delta J$$ (2.8)

where x_d denotes the depletion width, q stands for the elementary charge. The first term in eq. (2.8) is the leakage current density J_L, which is independent of time. The second term in eq. (2.8) is the transient signal of the current density δJ (t)), which is expressed as

$$\delta J(t) = -\frac{1}{2}qx_d N_T \frac{e_n}{e_n + e_p}\left(e_n - e_p\right)e^{-(e_n+e_p)t} = \begin{cases} -\frac{1}{2}qx_d N_T e_n e^{-e_n t} (e_n >> e_p) \\ \frac{1}{2}qx_d N_T e_n e^{-e_p t} \cong 0, (e_n << e_p) \end{cases} .$$ (2.6)

The amplitude of the transient signal δJ depends on the depletion width x_d, on the concentration N_T of deep traps and on the emission rate e_n. In order to achieve the efficient filling of deep traps and governing of a barrier in rather compensated material, the optical excitation is commonly employed for the high resistivity samples [3]. In the case of optical excitation, both majority and minority carriers determine the amplitude of the transient signal. Then, photo-injected carriers determine variations of depletion width

dependent on carrier drift velocity and on carrier concentration [7], due to carrier emission within partially depleted junctions. This leads to the more complicated transients.
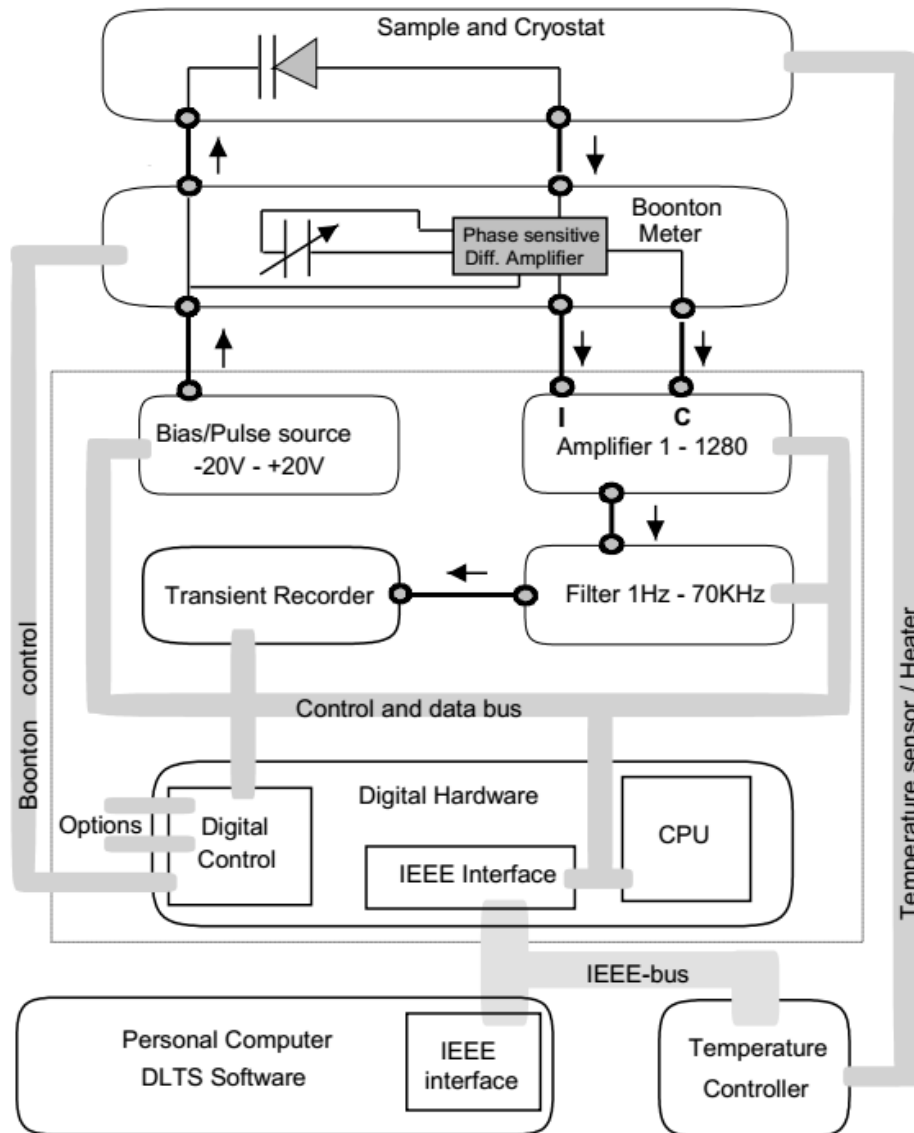

Fig. 2.5. HERA DLTS System 1030 spectrometer.

Deep level (DL) spectra over temperature range of 20-300K have been recorded on Schottky diode Si samples by employing transient spectroscopy (TS) technique implemented within a HERA-DLTS System 1030 spectrometer. The C-DLTS and current deep level transient spectroscopy (I-DLTS) measurements have been performed using either electrical (C-, I-DLTS) or optical (O-DLTS) carrier injection regimes, respectively. Optical excitation at 1064 nm wavelength has been implemented by pulsed (500 ms) radiation of a neodymium yttrium-aluminium-garnet (Nd:YAG) laser. The measurements and data sampling have been controlled using the PhysTech software installed within the HERA-DLTS System 1030 spectrometer, Fig. 2.5.
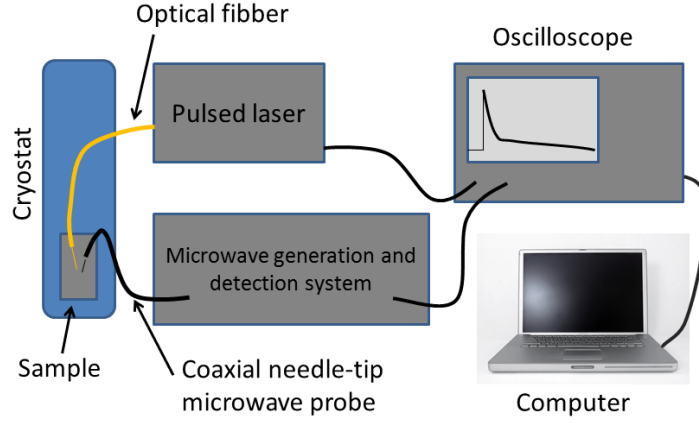
Fig. 2.6. TDTL spectrometer. VUTEG-6

Carrier thermal emission parameters have been alternatively examined by considering the temperature dependent carrier trapping lifetime (TDTL) within trapping component of transients recorded by microwave probed photoconductivity (MW-PC) technique. This technique is contact-less. Carrier trapping effect is recordable if two-componential carrier decay transients are observable at low excitation level. This decay process is characterized by an instantaneous decay lifetime expressed through [8] the recombination lifetime (τ_R) and the trapping coefficient K_{tr} as

$$\tau_{inst,tr} = \tau_R K_{tr}; \quad K_{tr} = 1 + \frac{N_{tr} N_{C,V,e,h,Ntr}}{(N_{C,V,e,h,Ntr} + \Delta n)^2}.$$

$$(2.9)$$

Here, N_{tr} is the concentration of shallow trapping centres, $N_{C,V,e,h,Ntr}= N_{C,V} exp(-E_{tr}/kT)$ is the effective density of band states for trapped carriers, and Δn is the excess carrier density which is involved into trapping. The latter model leads to a quasi-exponential decay, which is characterized by the time (t) dependent instantaneous lifetime $\tau_{inst,tr}(\Delta n(t))$. This model describes the excitation density and temperature dependent variations of the rate of the recombination-trapping process: recombination prevails within the initial stages of transients if $\Delta n >> N_{C,V,e,h,Ntr}$, N_{tr}. This trapping effect can thereby be verified by varying the excitation density when trapping effect is considerably suppressed at high excitation intensity. Also, the temperature (T) dependent variations of the trapping effect can be accounted for through $N_{C,V,e,h,Ntr}(T)$, $\Delta n(T)$.

The measurements of the temperature dependent carrier trapping lifetime (TDTL) have been performed by pulsed (400ps) excitation at 1062 nm wavelength using a coaxial needle-tip microwave (22 GHz) probe and a near field probing regime, performed by a proprietary measuring device VUTEG-6 (Fig. 2.6), fabricated at Vilnius University. This instrument contains temperature stabilization system for the temperature range from 80K to 400 K. A sample under investigation is routinely installed on a cold-finger within vacuum. The vacuum-proof step-motor arrangement is designed for the precise adjustment of the gap between the needle-tip probe and the sample placed on a cold-finger. The processed signal is transferred from the VUTEG-6 detection system to a digital 1 GHz oscilloscope Tektronix TDS-5104 equipped with a computer, where the MW-PC transients are displayed and analysed.

In the **III-rd chapter,** the obtained characteristics of carrier mobilities are represented and discussed. Theses characteristics have been examined on two sets of the bar-type samples with geometrical dimensions of 2 mm width, 6 mm length and 0.375 mm thickness. These sets contained the n-conductivity type (phosphorous-doped) and p-conductivity type (boron-doped) Si samples. The configuration of the electrodes for these samples exploited in Hall effect measurements is shown in the inset for Fig. 3.1. Additionally, a pristine sample prepared in Van der Pauw (VDP) configuration and being of 0.375 mm thickness and of 10×10 mm^2 area was invoked into Hall effect and magnetoresistance measurements. Samples were irradiated by 6.6 MeV electrons with fluences up to 5×10^{16} e/cm^2. The samples have simultaneously been examined using the steady-state Hall effect and magnetoresistance (MR) measurement techniques.

In the pristine samples, the characteristic (Fig. 3.1) of the temperature dependent Hall mobility is similar to that inherent for prevalence of the phonon-scattering processes. However, the Hall factor value for the whole temperature range should be known in order to evaluate the drift mobility. The geometry factor can also be a reason for uncertainties in evaluation of the drift mobility value. To overcome these uncertainties, the VDP geometry samples have been simultaneously examined with those used for Hall and magnetoresistance measurements. It has been obtained that the Hall mobility values, extracted using the VDP geometry and Hall geometry samples, lead to their ratio of 93%, as averaged over the whole range of examined temperatures. While, this ratio appears to be equal to 0.98 at low temperatures, 1.12 at 225 K and 1.1 at 300 K.

Irradiation should lower the carrier mobility because it creates the scattering and the charge compensation centres [3]. The ratio value of 1.15 (Fig. 3.4) between the magnetoresistance (MR) and Hall mobility values has been determined from characteristics of the Hall effect (Fig. 3.2) and magnetoresistance (Fig. 3.3). It is possible to infer that the MR effect can be employed to analyse the carrier drift mobility as both (MR and Hall) effects show the same dependence on temperature. This implies that measurements of the magnetoresistance can be employed for analysis of carrier mobility dependence on irradiation fluence also in the cases when the extended defects exist. The extended radiation defects raise the bulk inhomogeneity of samples, as it was observed in [9], as well as in [10, 11]. Due to bulk inhomogeneity, the Hall voltages are anomalously reduced by local space charge related electric field non-uniformities. Nevertheless, the magnetoresistance mobility still remains rather large, as revealed in [7-9]. In our experiments, the Hall mobility for the p-type samples significantly drops with increase of the irradiation fluence, as illustrated Fig. 3.5. It is known that the p-type silicon is less irradiation resistant than the n-type material. This is determined by impurities with the dandling bonds [12]. Then, the less irradiation energy is needed to break the molecular bonds. In our experiments, the magnetoresistivity (Fig. 3.6) characteristics indicate that the mobility is not so much suppressed by the irradiation. Nevertheless, the more detail consideration of the role of different carrier scattering mechanisms is necessary to understand carrier mobility changes under introduction of radiation defects.

Carrier mobility depends on the density of the ionized defects and the change of the mobility provides information about variations of the density of the scattering centres. It

has been approved that the Matthiessen's rule for the mobility is valid ($1/\mu=1/\mu_1+1/\mu_2+...$) for our experimental situations.
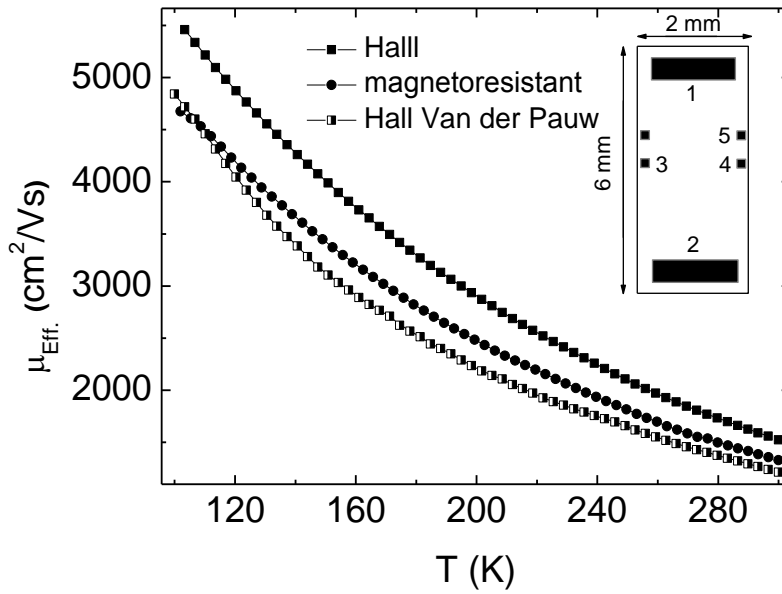

Fig. 3.1. Temperature dependent Effective mobility as a function of temperature in the pristine n-Si measured by Hall and magnetoresistence methods using bar-type Hall configuration and Van der Pauw geometry samples.
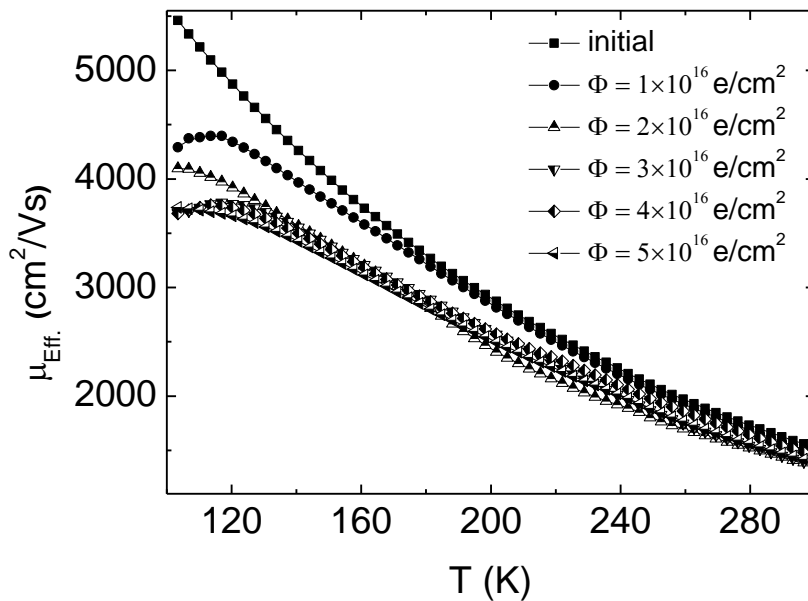

Fig. 3.2. Hall effective mobility as a function of temperature measured in the n-Si samples irradiated by 6.6 MeV electrons using different fluencies $(1, 2, 3, 4, 5) \times 10^{16}$ e/cm^2 and compared with values obtained for the pristine sample
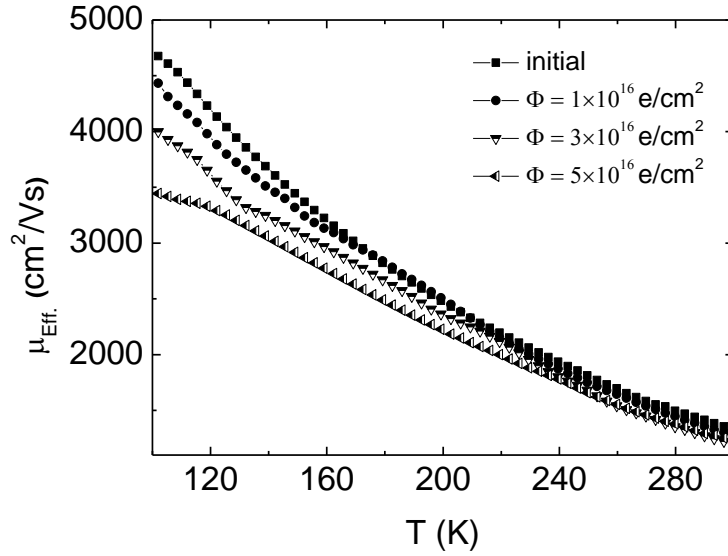
Fig. 3.3. Magnetoresistance mobility as a function of temperature measured in the n-Si samples irradiated by 6.6 MeV electrons using different fluencies $(1, 3, 5) \times 10^{16}$ e/cm^2 and compared with values obtained for the pristine sample.
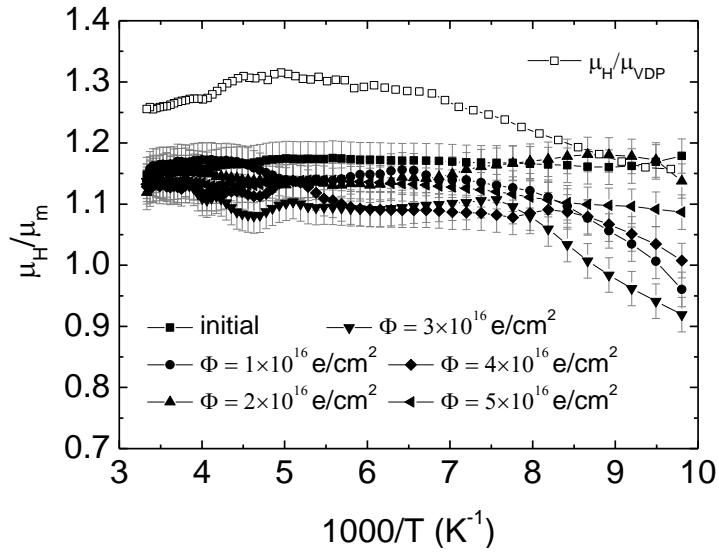

Fig. 3.4. The ratio of the Hall and magnetoresistance mobilities as a function of the reciprocal temperature measured in samples irradiated by 6.6 MeV electrons using different fluencies and compared with values obtained for the pristine sample, as denoted in the legend. The ratio between Hall mobility values measured in the bar-type (H) and Van der Pauw (VDP) configuration samples is additionally represented by open-square symbols.
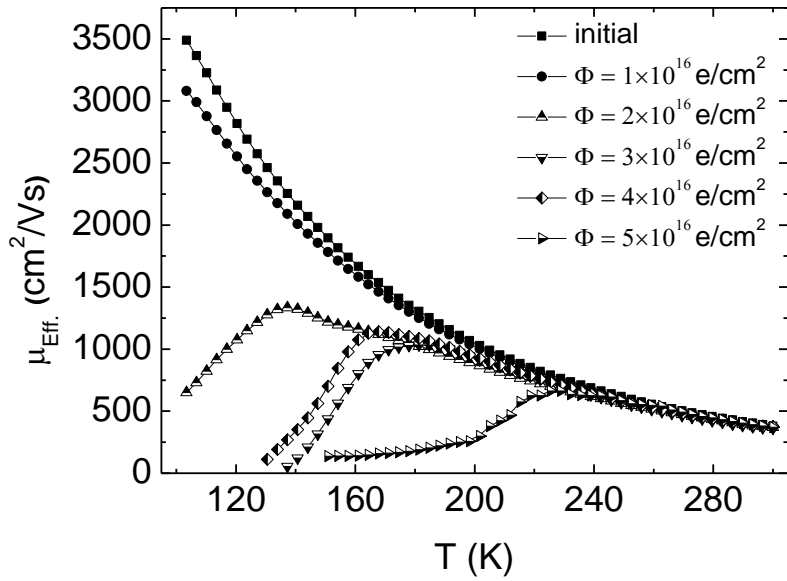
17

Fig. 3.5. Hall mobility as a function of temperature measured in the p-Si samples irradiated by 6.6 MeV electrons using different fluencies (1, 2, 3, 4, 5) $\times 10^{16}$ e/cm^2 and compared with values obtained for the pristine sample.
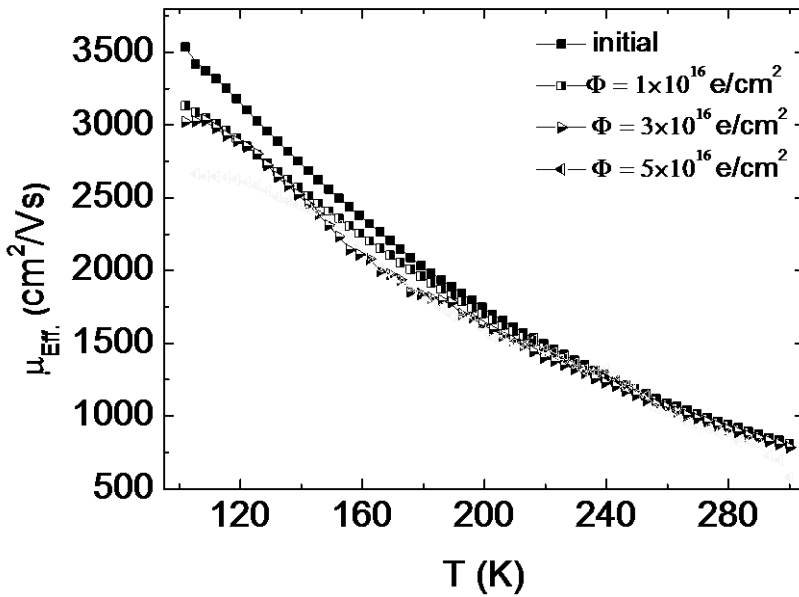

Fig. 3.6. Magnetoresistance mobility as a function of temperature measured in the p-Si samples irradiated by 6.6 MeV electrons using different fluencies (1, 3, 5) $\times 10^{16}$ e/cm^2 and compared with values obtained for the pristine sample.

The largest change of the mobility is determined by scattering centres ascribed to the radiation induced point defects acting as ionized centres. The predominant scattering by ionized centres leads to carrier mobility expression as

18

$$\mu = \frac{128\sqrt{2\pi}(\varepsilon\varepsilon_0)^2(kT)^{3/2}}{\sqrt{m}\ Z^2 e^3 N}F(N)$$

(3.1)

Here, all the parameters have common physical meaning and N stands for the density of these scattering centres. For the Conwell and Weiskopf model, the function *F(N)* is expressed as:

$$F(N) = \left(\ln\left[1 + \left\{ \frac{12\pi\varepsilon\varepsilon_0 kT}{Ze^3 N^{1/3}} \right\}^2 \right] \right)^{-1}.$$

(3.2)

While, for the Brooks and Herring model, this *F(N)* function is represented as

$$F(N) = \left(\ln[1+\xi] - \frac{\xi}{1+\xi} \right)^{-1}$$

(3.3)

with

$$\xi = \frac{96\pi^2\varepsilon\varepsilon_0 m}{N}\left(\frac{kT}{he} \right)^2$$

(3.4)

The change of density of these scattering centres *N* with the irradiation fluence is the most important characteristic to estimate the type and the role of radiation defects. By using the Matthiessen's rule, the impact of the phonon dominant scattering can be eliminated within analysis of radiation induced scattering centres by exploiting mobility values obtained for the pristine samples where phonon mechanism is prevailing. Non-linear equations were solved for each temperature-scan (*T*) point, and the simulation/fitting results are presented in Fig.3.7–3.8.

Fits between simulated and experimental data obtained using the mentioned models (eq. (3.2)) and (eqs. (3.3-3.4)) do not change the shape of the characteristics. The only difference appears in absolute values calculated using these models, where 10 times smaller mobility values have been obtained Conwell and Weiskopf (eq. (3.2)) model. Nevertheless, Brooks and Herring model is more reliable because it includes screening effects, which should be taken into account for doped and rather electrically conductive materials. Both experimental characteristics obtained by Hall and magnetoresistance techniques were exploited for extraction of the density of the ionized scattering centres *N*, and as a measure for the reliable evaluation of this *N* density served the coincidence of the regions with equal Hall and magnetoresistance mobility values

Variations of the density of the ionized scattering centres *N* as a function of the reciprocal temperature showed the exponential behaviour segments with activation energies at least twice smaller than those inherent for thermal emission from A-centres or di-vacancies. Also, *N* values do not correlate with density of excess carriers, as illustrated in Fig. 3.9. This fact suggests that not all ionized centres are involved into the scattering process, i.e. significant amount of dopants are screened by other defects (the screening by free carriers has already been accounted for). This implies that space charge regions associated with these defects overlay and interact through the electrostatic fields. The uncertainties of spread of these regions determine the systematic errors within simulations of carrier mobility values. Thus, mobility measurements allowed only estimation of the lowest limit for the total density of defects. These estimations lead to the ionized centre density values of 5×10^{12} and 1×10^{13} cm^{-3} for n-Si and p-Si samples,–

respectively. Additionally, the activation energy values from 44 meV to 86 meV extracted from N vs. T^{-1} characteristics correspond to the potential barriers.
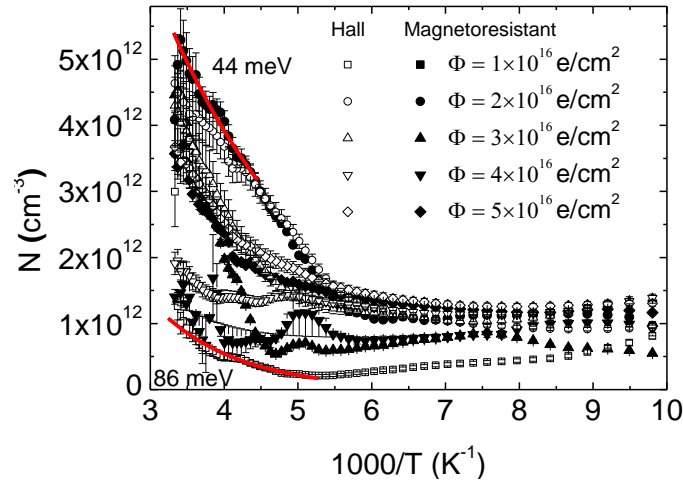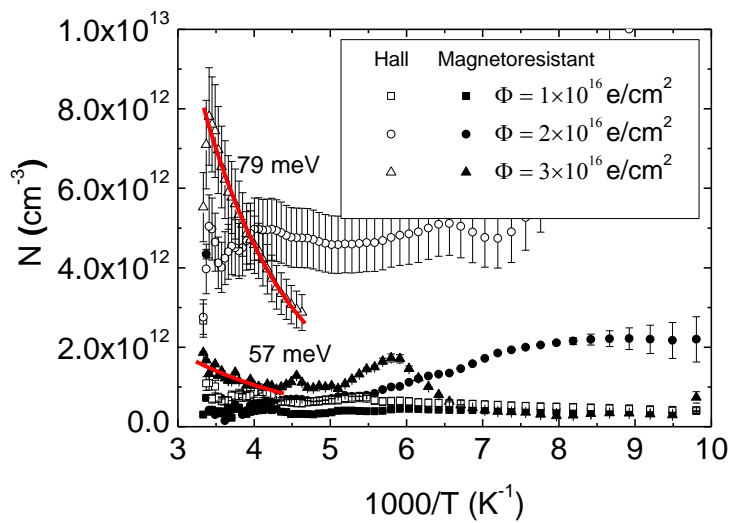

Fig. 3.7. Density of ionized defects as a function of reciprocal temperature evaluated using temperature dependent carrier mobility characteristics measured in n-Si samples irradiated with 6.6 MeV electrons of different fluencies, as: (1, 2, 3, 4, 5) $\times 10^{16}$ e/cm^2. Solid lines represent the exponential segments involved into fitting procedures for extraction of barrier thermal activation energy.

Fig. 3.8. Density of ionized defects as a function of reciprocal temperature evaluated using temperature dependent carrier mobility characteristics measured in p-Si samples irradiated with 6.6 MeV electrons of different fluencies, as: (1, 2, 3, 4, 5) $\times 10^{16}$ e/cm^2. Solid lines represent the exponential segments involved into fitting procedures for extraction of barrier thermal activation energy.

Equilibrium carrier density is routinely evaluated using the electrical conductivity and carrier mobility data which are measured separately. This carrier density has been evaluated for the pristine samples to be $(1-2)\times 10^{15}$ cm^{-3} (n-Si and p-Si materials). Irradiations modify these values by introduction of insulating (or compensated) regions, which are not excluded from the density calculations when the averaging is performed over whole sample volume. The local density of the conductive regions may there

remain almost the same as in the non-irradiated samples. Characteristics of the temperature dependent carrier density variations (Fig. 3.9) can serve for evaluation of thermal activation energy attributed to different radiation induced defects. Thereby, it has been obtained slopes within temperature dependent carrier density variations (Fig. 3.9) with thermal activation energy of 0.19 and 0.4 eV. These activation energy values are well-known for irradiated Si materials and correspond to A -centres and either to di-vacancies or vacancy-boron pairs, respectively.
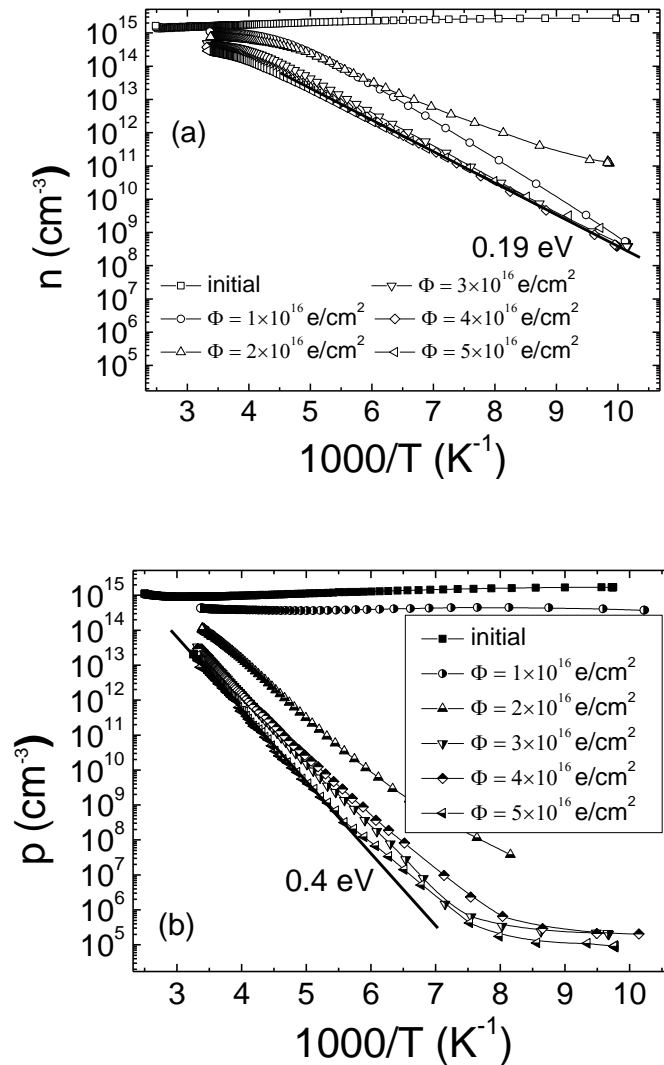

Fig. 3.9. Equilibrium carrier density as a function of reciprocal temperature in n-Si (a) and p-Si (b) samples of pristine materials and that irradiated with 6.6 MeV electrons of fluences (1, 2, 3, 4, 5) $\times 10^{16}$ e/cm^2.

Electrons of 6.6 MeV energy with 0.2 cm [13] stopping depth in Si are penetrative for the examined samples of d=0.375 mm thickness. Thus, the average energy involved into creation of radiation defects over the whole sample thickness comprises value of $6.6 \times (1 - \exp(-0.0375/0.2)) = 1.1$ MeV. The number R of created defects (of density N in sample volume $V=Sd$ (of surface area S under irradiation with fluence Φ) by each irradiation particle is estimated as $R = \Phi S/(NV) = \Phi/(Nd)$. The density N of scattering

centres is independently evaluated using mobility data, and the energy required for creation of a single defect is determined as $1.1\text{MeV}/R = 1.1\text{MeV} \times Nd/\Phi$. The obtained energy values as a function of fluence calculated for n-Si and p-Si materials are illustrated in Fig. 3.10. It can be inferred that the characteristic energy for single defect creation in n-Si material is a few times larger than that for in p-Si in the range of the lowest irradiation fluences, while these values coincide for n-Si and p-Si in the range of the highest fluences.

The number R of created defects can alternatively be estimated by analysis of Frenkel pair creation. The electron of averaged 1.1MeV energy produces 88000 point defects in silicon sample, when it is assumed 12.5 eV energy necessary for single Frenkel pair creation. The density of point, Frenkel-pair-type defects is obtained to be $(3.03; 6.06; 9.09; 12.1; 15.2) \times 10^{12}$ cm^{-3} under irradiation with fluences of $(1, 2, 3, 4$ and $5) \times 10^{16}$ cm^{-2}, respectively. The density of the neutral and ionized carrier scattering centres can be distinguished using measured mobility values. The density of ionized defects had been evaluated using procedures of fitting between experimental and simulated (using Brooks-Herring approach) mobility data. Then, the highest density of neutral carrier scattering centres can be estimated by subtraction of the density of the ionized defects from the total amount of scattering centres. Theses estimations are illustrated in Fig .3.11, by representing the defect densities as a function of irradiation fluence. The obtained increase of radiation defect density N with fluence routinely confirms the crystal structure damage. The characteristics illustrated in Fig. 3.11 also imply defects, created under irradiations above certain fluence, are located rather close to each other and behave like as clusters.
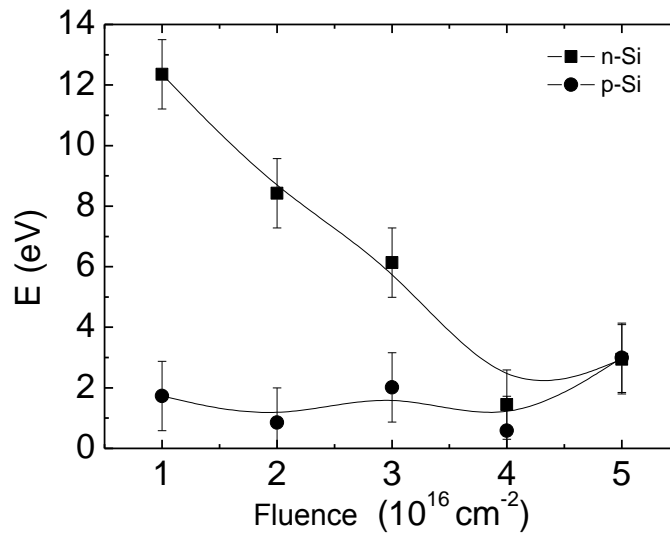

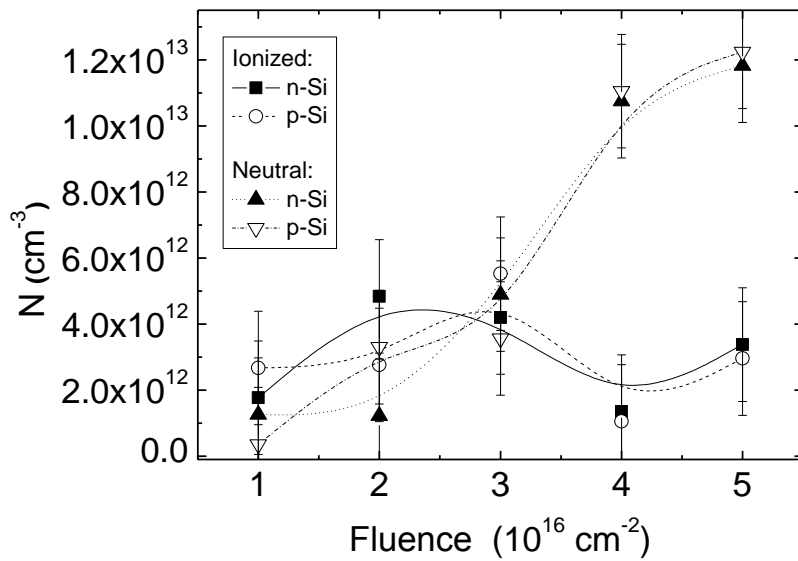Fig. 3.10. Defect creation energy as a function of irradiation fluence calculated for n-Si and p-Si materials.

Fig. 3.11. Density of point defects acting as carrier scattering centres (neutral or ionized) as a function of irradiation fluence.

The threshold fluence of 8×10^{16} cm^{-2} to reach the overlap of space charge regions, ascribed to radiation clusters, has been estimated by linearly extrapolating the Hall voltage maximal values dependent on temperature and fluence.

In the **IV-th chapter** variations of the carrier scattering and emission characteristics induced by reactor neutron irradiations are considered. Si samples were irradiated by fluences in the range from 10^{12} n/cm^2 to $3 \cdot 10^{16}$ n/cm^2.

It has been revealed that the simple scattering centre model is not valid for the samples irradiated with the higher fluences than 1×10^{14} cm^{-2}. The probable carrier scattering processes can be clarified by the analysis of the mobility temperature variations (Fig.4.1). The decrease of the Hall mobility with enhancement of the neutron irradiation fluence was observed in the preceding article [14] and explained by proposing the model of the insulating sphere cluster [15]. As this cluster model is multi-parametric, the Hall and magnetoresistance mobilities and their dependences on temperature and fluence should be considered to complete the description model.

The magnetoresistance mobility dependence on temperature is similar to that predicted [16] for the case of carrier scattering on the macro-inhomogeneities (clusters). There, the mobility dependence on temperature can be approximated by the proposed [14] linear dependence on temperature (Fig.5.1a). In the 10^{12}-10^{13} cm^{-2} neutron fluence irradiated and annealed samples (Fig.5.1b), the mobility value at room temperature is not far away from that simulated for the phonon scattering mechanism. Therefore, it is reasonable to analyse contributions of all the possible scattering processes using the Matthiessen's rule. The mobility dependence on temperature is here approximated by a function of type $\mu = a_i T^{\alpha}$, where power index α depends on the scattering mechanism. Using the mentioned approach, the obtained simulation (shown in figures by solid lines) and fitting results can only be used for the qualitative description of the characteristics. This is determined by the multi-parametric problem and rather large experimental errors.

Nevertheless, these simulations enabled us to evaluate contributions of scattering processes described using low positive and negative α values in fitting procedure.
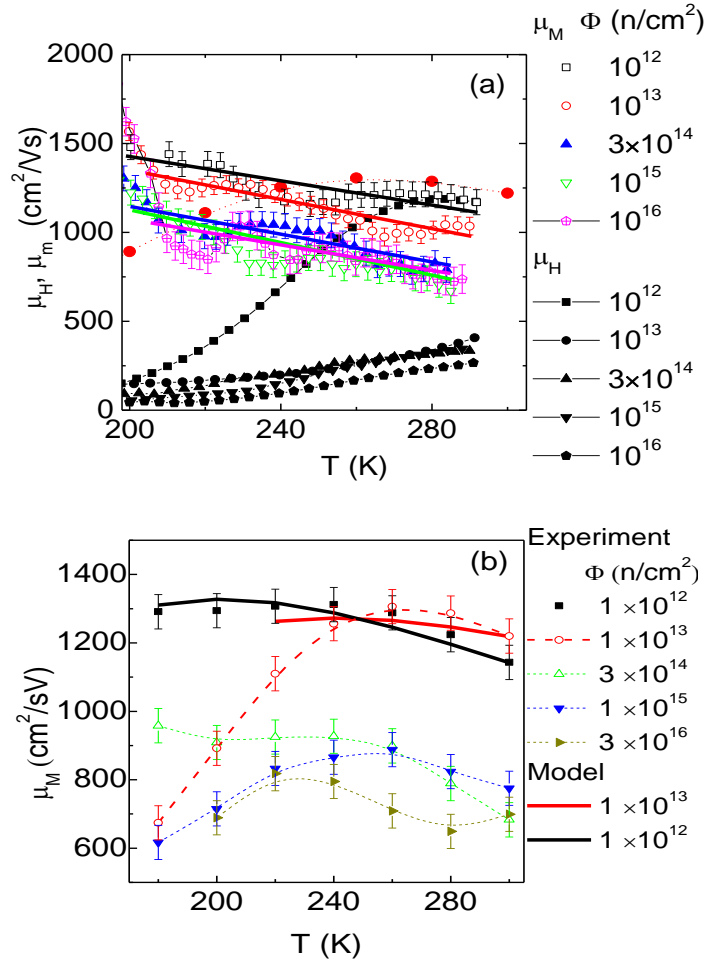

Fig. 4.1. Hall and magnetoresistance mobility as a function of temperature in the neutron irradiated Si samples. a – mobility characteristics obtained on the as–irradiated high resistivity Si samples. Here, the solid lines represent averaging with linear approximation over the range of experimental errors. b – magnetoresistance mobility obtained for the neutron irradiated and 24 h annealed at 80⁰C the same Si samples. Here, solid lines represent the simulated characteristics.

The temperature dependence of the carrier concentration has been evaluated by combining the measured values of mobility and conductivity. These characteristics obtained for samples irradiated with different fluences are illustrated in Fig. 4.2.

There, contribution of different deep levels has been evaluated using classical approaches [17]. The role of different deep levels depends on the position of the Fermi level [18]. The partially compensated semiconductor approximation has been employed when Fermi level (E_F) resides below the defect level. Then equilibrium carrier density is related to the parameters of localized deep and continuum states as:

$$n = (N_M - N_K)/[1 + (\beta N_K / N_C)\exp(\Delta E_M / kT)].$$

(4.1)

Here, N_M is the deep level concentration, N_C is the density of states in the conduction band, β the deep level degeneration factor, ΔE_M is the deep level activation energy, k is the Boltzmann constant and N_K is the concentration of the compensating deep centres. The non-compensated semiconductor model [18] has been exploited when Fermi level is at or above the deep level. This leads to expression for equilibrium carrier density as:

$$n = N_M / [1 + \sqrt{1 + (4\beta N_M / N_C)\exp(\Delta E_M / kT)}]$$

(4.2)

Concentrations and activation energies of different deep levels have been extracted by employing the above (4.1) and (4.2) approximations and fitting the temperature dependent variations of equilibrium carrier concentrations (Fig. 4.2). Variations of concentration of different deep levels with neutron irradiation fluence are presented in Fig. 4.3.
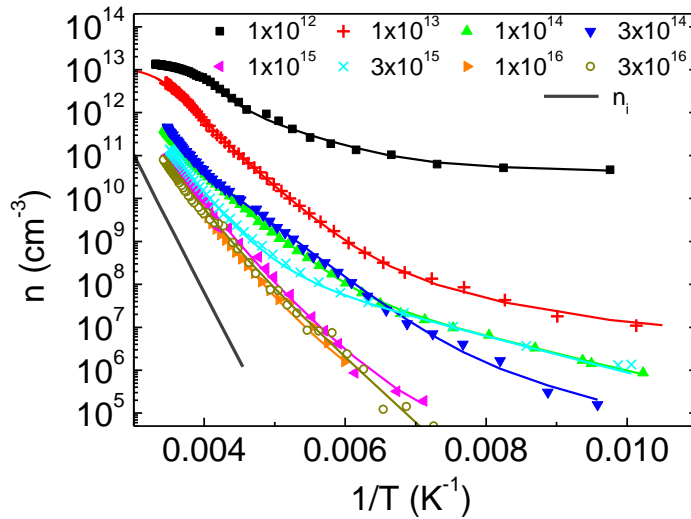

Fig. 4.2. The electron concentration as a function of reciprocal temperature evaluated for samples irradiated with different neutron fluences. The solid lines represent the simulated and fitted to the experimental data characteristics.

By analyzing the characteristics represented in Figs. 4.2 and 4.3, several features have been unveiled. For the Si samples irradiated by a 10^{12} cm^{-2} fluence in the range of low temperatures, very weak carrier concentration dependence on temperature is obtained. This indicates the concentration of fully ionized shallow centres which are not compensated by deep levels of density 5×10^{10} cm^{-3}. For the elevated temperature range, the activation energy of the prevailing centres is comparable with the Fermi level distance from the conductivity band. The activation energy of 0.22 eV for these centres has therefore been determined using relation (4.2). To fit to the experimental data, it has been revealed necessity to include a contribution of the deeper level. Then, activation energy of 0.36 eV has been extracted by fitting carrier concentration described by relation (4.1). The extracted activation energy values of 0.36 eV and 0.22-0.23 eV are inherent [19] for irradiated Si materials. The deep centres with these activation energies are often attributed to tri- and di-vacancies, respectively. The contribution of the

additional shallow centres, with activation energy of 70 meV, has been revealed. The latter centres are also associated with tri- and di-vacancies [16]. The same set of the levels has been kept in fitting of all the characteristics, shown in Fig. 4.2, for the fluence range of 10^{12}-10^{14} cm^{-2}, to avoid uncertainties caused by usage of too many free parameters. More complicated situation appears in fitting of the experimental characteristics for the range of >10^{14} cm^{-2} fluences. The activation energy has been found to be depended on the fluence for the range of >10^{14} cm^{-2} fluences. This indicates the indirect interaction between the radiation centres. The absence of the direct interaction for the range of >10^{14} cm^{-2} fluences had been demonstrated in [20]. There, the generation current linear dependence on fluence had been obtained in the irradiated diode structures.
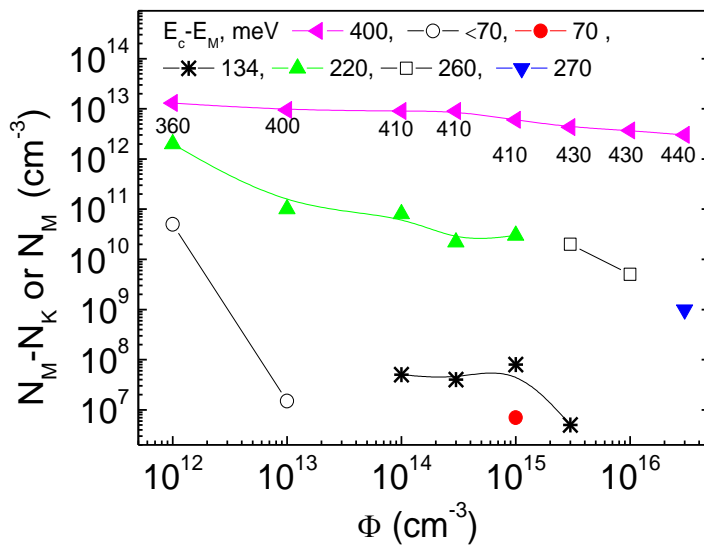

Fig. 4.3. The concentration of deep levels (extracted by fitting the experimental characteristics of temperature dependent carrier concentrations, described by expressions (4.1) and (4.2)) as a function of neutron irradiation fluence. Activation energy values ascribed to different centres are denoted in figure legend.

The photo-ionization spectroscopy is a powerful tool for separation of electrically active centres introduced by irradiations. Investigation of photo-ionization phenomena in the irradiated Si materials, grown using various (as MCZ, FZ and epitaxial) techniques, has showed that in samples, irradiated with low and moderate fluences, the photo-response is independent of the photo-ionization measurement regime, when using either enhancement or reduction of photon energy to obtain a photo-ionization spectrum. The photo-ionization spectra for this sample sets exhibit only weak dependence on temperature. However, in several sets of Si samples, especially irradiated with elevated fluences, the hysteresis effect in spectra variations is clearly pronounced, (Fig. 4.4) where photo-response signal crucially depends on sequence of the wavelength varied photo-excitation cycling. As illustrated in Fig. 4.5, the photo-current exhibits lower values when the photon energy is increasing, while it features the elevated values when the photon energy is decreasing. Additionally, the repeated measurements do not

reproduce the same spectral curves, and the enhanced current values are obtained in every next cycle of spectrum recording. The re-arrangement of experiments by employing background steady-state illumination together with wavelength varied photo-excitation showed no impact of long thermal emission (responsible for relaxation effects) and of trap filling (by varied background illumination intensity). Therefore, to clarify features of this photo-response hysteresis in the irradiated Si samples, the spectral photo-ionization measurements were performed by cycling regime each time with different maximal photon energy till the photo-current saturates and spectral curve shapes reach a convergence. It has been additionally revealed, that annealing may also enhance the observed hysteretic effect, as illustrated in Fig. 4.6.
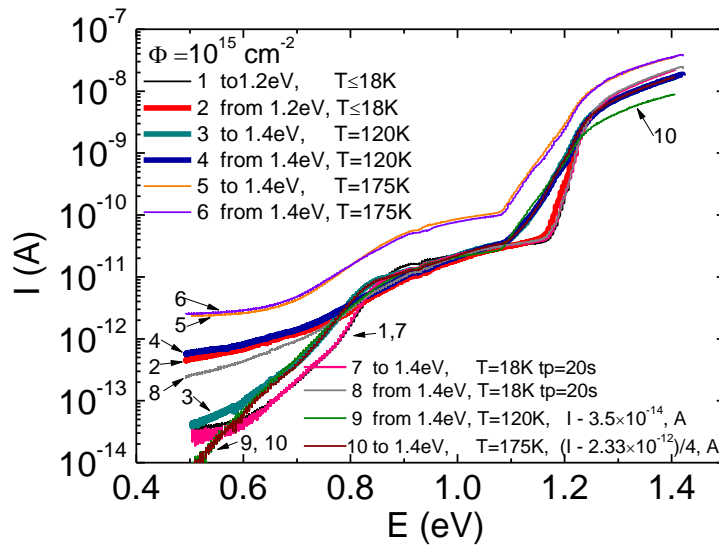

Fig. 4.4. The photo-current as a function of photon energy recorded by increasing and decreasing of a photon energy to get photo-ionization spectrum in epitaxial Si diode sample, where the hysteresis effect is weak.
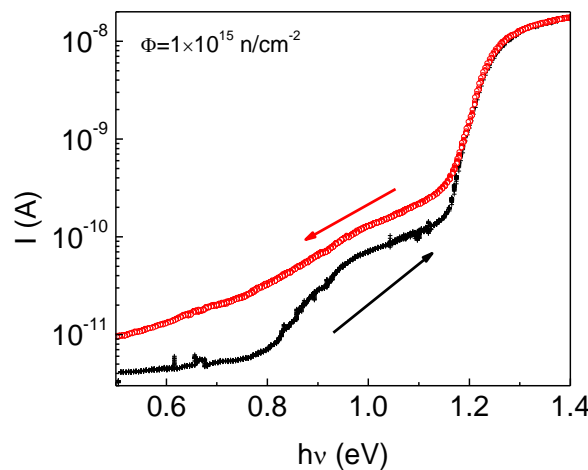

Fig. 4.5. The photo-current as a function of photon energy recorded by increasing and decreasing (arrows show the tendency of the photon energy change) of a photon energy to get photo-ionization spectrum in the neutron irradiated MCZ Si sample with ohmic contacts.
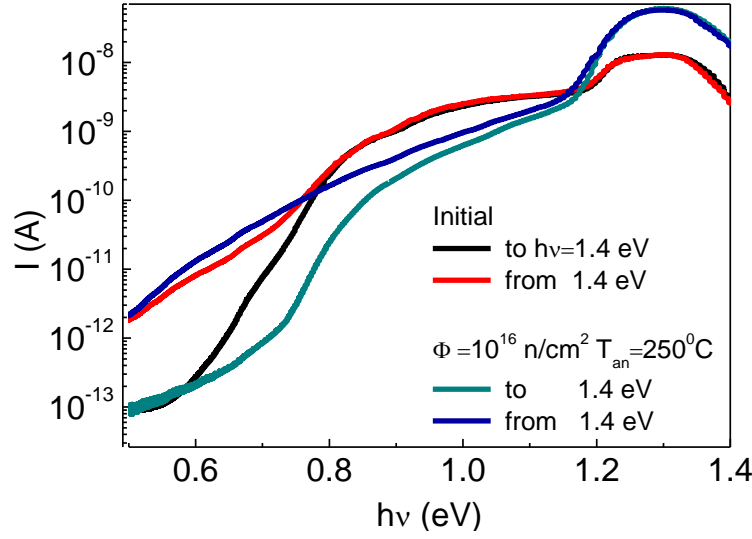
Fig. 4.6. The photo-current as a function of photon energy recorded by increasing and decreasing of photon energy to get photo-ionization spectrum in the neutron irradiated FZ Si diode sample.

The photo-ionization spectra have been considered and interpreted using the Lukovsky model [1], where a spectral-steps, attributed to the photon-electron interaction cross-section $\sigma(h\nu)$ spectral changes, are observed and described by a power-law function. The Lukovsky model is applicable when the electron-phonon interaction can be ignored. This model is suitable for analysis of the photo-ionization spectra applied to point defects [22]. In the case of strong the electron-phonon interaction, the photon-electron interaction cross-section $\sigma(h\nu)$ is proportional to the convolution integral with Gaussian function [7], and expressed as

$$\sigma(h\nu) \propto \frac{1}{h\nu} \exp\left(-\frac{(h\nu - E_0)^2}{A^2}\right) \qquad (4.3)$$

The radiation cluster-type defects contain potential barriers, which may separate photo-excited electrons and holes. This causes the accumulation of charge and formation of space charge regions, and redistribution of local electric fields lead to the prolonged relaxation of photo-current. This relaxation can be modified by the small-step enhancements of the photon energy up to photo-current saturates Then, the photo-current increase between the neighbour steps is proportional to the difference of the optical cross-section. This differential photo-response may be approximated by spectral derivative of the photon-electron interaction cross-section $\sigma(h\nu)$ as:

$$\Delta I(h\nu) \propto \frac{d\sigma(h\nu)}{d(h\nu)} \qquad (4.4)$$
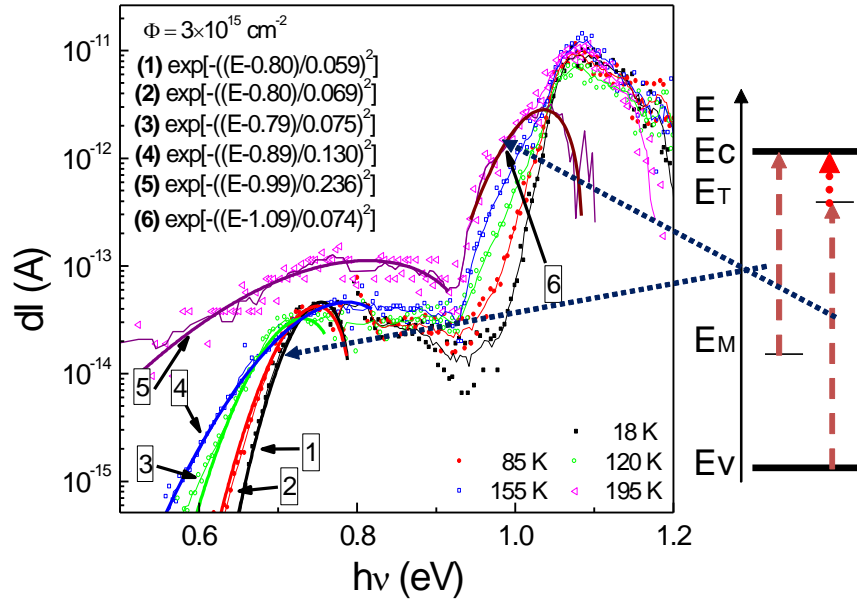
28

Fig. 4.7. The experimental and simulated photo-ionization spectral steps recorded in MCZ Si diode at different temperatures. The energy diagram of photo- and thermally activated transitions is sketched on the right of picture. The Gaussian function parameters are denoted in the legend.

Simulations of the photo-ionization spectra obtained for rather heavily irradiated Si structures have been performed employing the approaches expressed by (4.3) and (4.4) relations. The fitting of the experimental spectra by simulated spectral steps using the (4.3) and (4.4) relations is illustrated in Fig. 4.7.

On the basis of analysis of the photo-ionization spectra and the photo-current relaxation and hysteresis characteristics, the two-channel photo-ionization process model has been created. One channel includes the direct optically excited transitions from the level (E_M) with activation energy varied from 0.8 eV to 1 eV with temperature increase. The parameters for this, the first channel have been evaluated using Gaussian fits (eq. (4.4)). By taking into account the temperature dependent bandgap variations for Si material and the level approach to the valence band (E_V) with temperature increase, it has been concluded that this (0.8 - 1 eV) energy level is formed from the valence band states. Another carrier excitation channel is realized by two-transitional process including subsequent thermally excited (E_T) electron transition, as sketched in Fig. 4.7. For heavily irradiated Si materials formation of shallow donors is less probable [23], therefore photo-ionization process happens through the empty level (E_T) within the second channel. This E_T level is close to the conduction band (E_C). Therefore, the second channel process is a reasonable model to explain the experimental observations of the temperature dependent photo-activation energy. Then, the photon capture cross–section is described by the Gaussian shape function. Carrier recombination (via this centre) transforms all the energy to the crystal lattice due to the strong electron-phonon interaction. These

processes can be a reason for the recombination enhanced transform of the defect, similarly to the model proposed in [22].

In the **V-th chapter** the thermal activation processes and their parameters in heavily irradiated Si structures are considered and radiation defect transformations under thermal treatments are discussed. The Schottky diodes and ohmic contacts containing Si structures irradiated by 6.6 MeV electrons with fluences up to 5×10^{16} e/cm^2 have there been investigated

The combined study of carrier thermal emission spectra using deep level transient spectroscopy (DLTS) and temperature dependent trapping lifetime (TDTL) spectroscopy (implemented by contact-less microwave probed photo-conductivity (MW-PC) transients) techniques appeared to be the effective tool for the identification and spectroscopy of the radiation defects in heavily electron irradiated Si. The correlations between the DLTS and MW-PC spectral signatures enabled us to trace radiation defect transforms in heavily electron-irradiated samples of CZ n-Si with doping concentrations in the range of 10^{15} cm^{-3}.
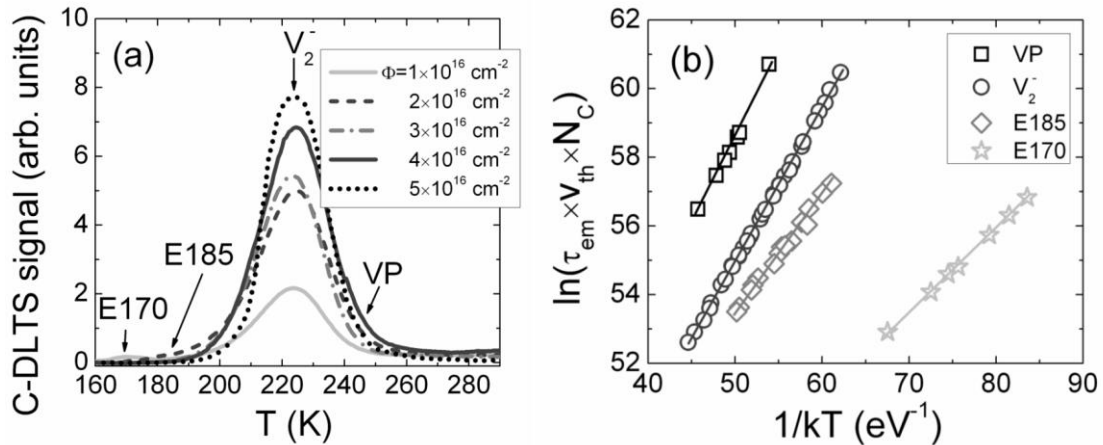

Fig. 5.1. Evolution of the C-DLTS spectra with irradiation fluence recorded on n-Si Schottky diodes (a) and the corresponding Arrhenius plots for traps resolved in sample irradiated with fluence of $\Phi = 1 \times 10^{16}$ e/cm^2 (b).

The radiation induced defects, ascribed to vacancy-oxygen (*VO*) and interstitial Si-oxygen (*IO₂*) complexes, to agglomeration of vacancies *A-V*, to vacancy-phosphorus (*VP*) complexes, and to non-identified defects (labelled as *E170, E185, I120, I180, I205*), have been observed in the irradiated non-annealed samples by C-DLTS and I-DLTS spectroscopic techniques (Fig. 5.1). It has been obtained that the amplitudes of the di-vacancy and the *I180* centre ascribed peaks increase with enhancement of irradiation fluence, Fig. 5.2.
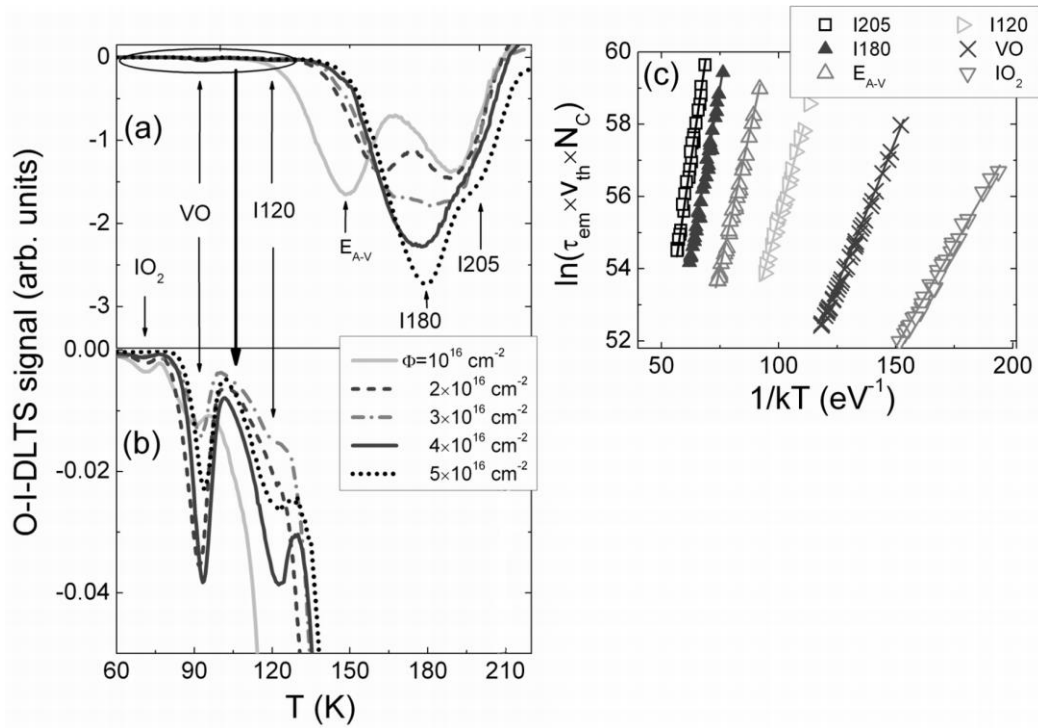
Fig. 5.2. Variations of the O-I-DLTS (a, b) spectra dependent on irradiation fluence. Here, figure (b) represents the low temperature spectral wing in more detail. The Arrhenius plots obtained for different separated spectral peaks are illustrated in figure (c) for sample irradiated with fluence of $\Phi = 1 \times 10^{16}$ e/cm^2.
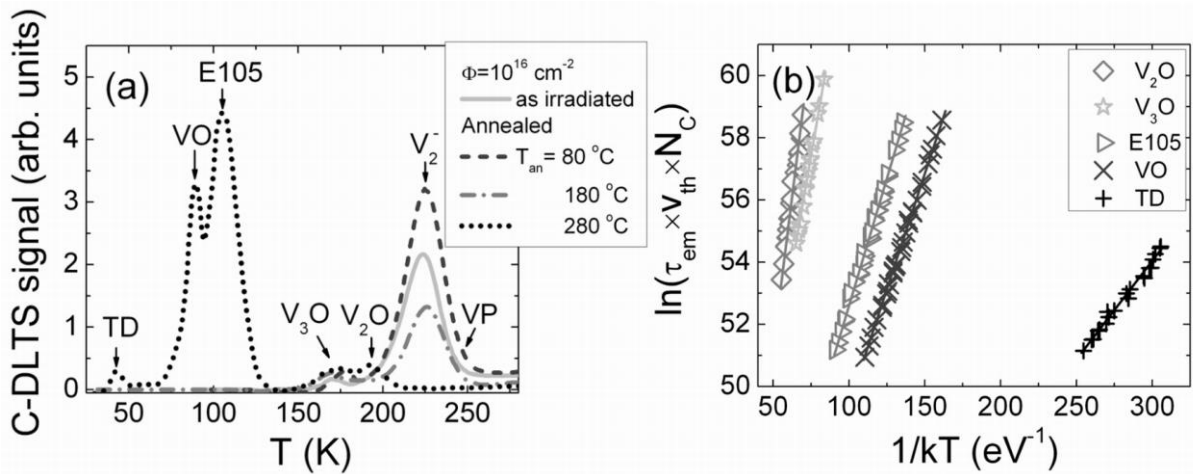

Fig. 5.3. a- C-DLTS spectra dependent on annealing temperature recorded on Schottky diodes irradiated with fluence of $\Phi = 10^{16}$ e/cm^2. b- The Arrhenius plots obtained for different spectral peaks obtained in these Schottky diodes annealed at 280°C.
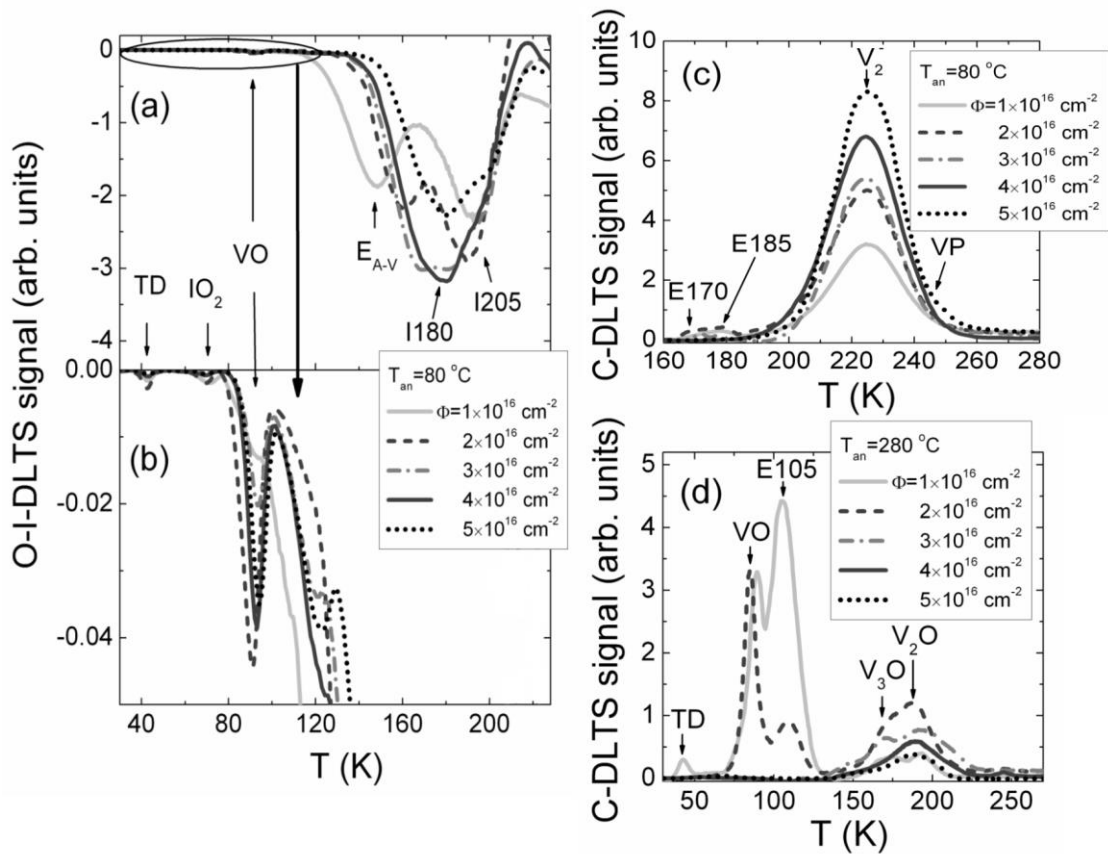
Fig. 5.4. Comparison of variations of the O-I-DLTS (a, b) and C-DLTS (c, d) spectra dependent on irradiation fluence for diodes heat-treated at T_{an}= 80°C (a, b, and c) and 280°C (d) temperatures. Here, figure (b) represents a fragment of the O-I-DLTS spectrum within low temperature wing.
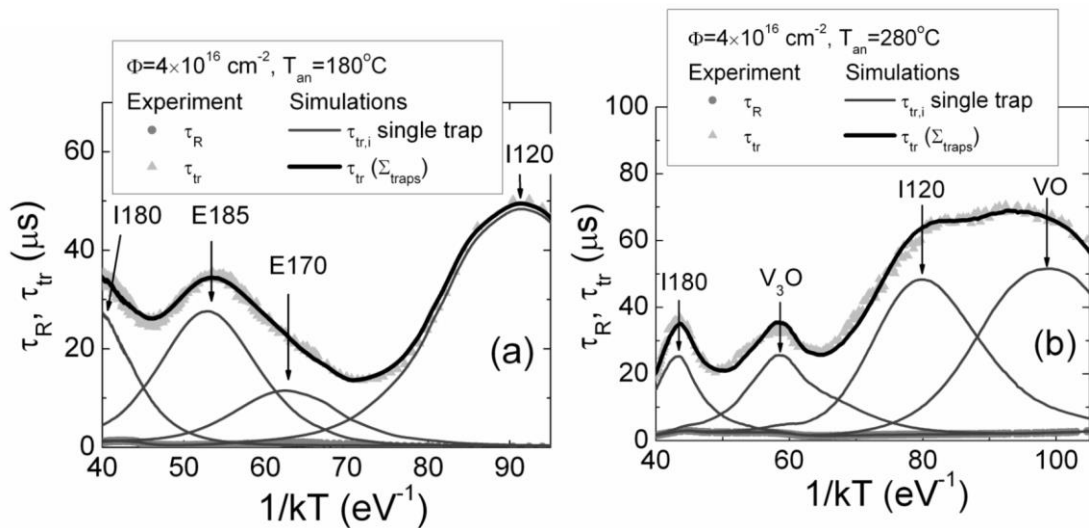
Fig. 5.5. Comparison of the simulated (curves) and experimental (symbols) variations of the carrier trapping lifetimes (τ_{tr}) as a function of reciprocal thermal energy for samples irradiated with fluence of 4×10^{16} e/cm^2 and annealed for 24 h at temperatures T_{an}=180°C (a) and T_{an}=280°C (b). Here, the bold curve represents a sum of emission flows from different trapping levels those form the single thermal emission peaks, shown by thin solid curves. Simulations of the resultant $\tau_{tr}(T)$ spectrum were performed including temperature dependent changes of the recombination lifetime $\tau_R(T)$.

It has been obtained that annealing at 80°C leads to the increase of the *VO, E170, E185* and *I180* defect density. As predicted, the annealing out of the *VP* defect has been detected after annealing at 180°C (Fig. 5.3). The heat treatment at the highest applied temperature of 280°C leads to the considerable transformation of these defects, as follows: the peaks attributed to *VO* and to *E105* defects prevail in samples irradiated with rather moderate fluences of $\Phi \leq 2 \times 10^{16}$ e/cm^2. While, the irradiation by elevated fluences of $\Phi \geq 3 \times 10^{16}$ e/cm^2 leads mainly to prevailing of the more intricate vacancy-oxygen complexes *V$_3$O* and *V$_2$O,* as can be deduced from Fig. 5.4. The benefit of heat treatment using elevated temperatures has been revealed through the reduction of concentration of the deep centres (*V$_2^-$* and *VP*). However, this suppression of deep traps is accompanied by the increase of the shallow acceptor concentrations, attributed to the accelerated formation of *E105* defect. This implies dissociation of radiation induced vacancy complexes such as *VP* and *V$_2^-$*. An enhancement of the concentration of these shallower acceptor-type traps determines nevertheless the dopant compensation effects and degrades the diode barrier characteristics.

The complicated experimental spectra, recorded using DLTS and MW-PC techniques, of carrier recombination and thermal emission lifetimes have been fitted using the simulated characteristics of τ_R*(1/kT)* and τ_{tr}*(1/kT).* The contact-less MW-PC technique allowed identifying of the trapping centres in the heavily irradiated samples after heat treatment at $T_{an} \geq 180$°C. These trapping centres have been ascribed to *I180, E185, E170, V$_3$O, I120,* and *VO* defects, respectively, in agreement with DLTS spectroscopy data (Fig. 5.5).

It has been demonstrated that the contact-less MW-PC measurements and TDTL analysis can be a preferential tool to reveal the interplay of several radiation defects.

Conclusions

1. The ratio between the Hall and magnetoresistance mobilities of value 1.15 has been determined for reliable measurements of the carrier scattering parameters in heavily irradiated Si materials. It has been revealed that magnetoresistance effect is less sensitive to material micro-inhomogeneities than the Hall effect. Therefore, magnetoresistance measurement technique is preferential for analysis of properties of semiconductors with the extended defects.

2. Heat treatments of the heavily electron irradiated Si structures lead to the decrease of the deep acceptor concentrations due to transformations of the defects, which is followed by enhancement of the shallow acceptor concentration attributed to the accelerated formation of the *E105* defects.

3. Two carrier excitation mechanisms are competing within photo-ionization processes in silicon irradiated by high fluencies. The optically excited transitions from deep centres, the photo-activation energy of which enhances from 0.8 eV to 1.0 eV and depends on temperature, prevail within the first channel. Another mechanism is the two-stage sequence process which includes photo-ionization events and thermal activated transitions.

4. The radiation induced centres with the typical activation energy of 0.22–0.23 eV and of 0.36 eV prevail in carrier scattering processes. These centres have been ascribed to formation of di-vacancies and tri-vacancies in Si structures irradiated with larger fluences.

5. Tunnelling efficiency from the radiation cluster states depends on a width of the potential barrier, which is related to Debye length within space charge region surrounding the cluster. Neutron irradiation induced defects reduce the bulk electrical conductivity of material, so the Debye length there increases, and the higher thermal energy is needed for carrier tunnelling from the cluster.

6. Different species of traps and paths of their transformations under anneals have been identified in large fluence ($\geq 10^{16}$ cm^{-2}) irradiated silicon using correlations of DLTS and TDTL spectra.

7. Contact-less spectroscopy of carrier recombination and trapping lifetime temperature variations allows simultaneous control of interactions among several radiation defects in large fluences irradiated Si structures. This technique is promising for spectroscopy of radiation defects in large fluence irradiated Si when the standard contact methods become unsuitable due to the disordered structures and internal electric fields existing within heavily radiation damaged materials.

References

[1] G. Lucovsky, Solid State Communications, (1965) 299-302.

[2] P. Blood and J. W. Orton, The electrical characterization of semiconductors: majority carriers and eletron states, Academic Press Inc., San Diego (1992).

[3] D. V. Lang, Deep-level transient spectroscopy: a new method to characterize traps in semiconductors, J. Appl. Phys. **45** (1974) 3023.

[4] S. U. Pandey, P. Middelkamp, Z. Li and V. Eremin, New experimental and analysis methods in I-DLTS, Nucl. Instrum. Meth. Phys. Res. A **426** (1999) 109.

[5] E. Gaubas, D. Bajarūnas, T. Čeponis, D. Meškauskaitė and J. Pavlov, Optically induced current deep level spectroscopy of radiation defects in neutron irradiated si pad detectors, Lith. J. Phys. **53** (2013) 215.

[6] Z. Li, Systematic modelling and comparisons of capacitance and current-based microscopic defect analysis techniques for measurements of high-resistivity silicon detectors after irradiation, Nucl. Instrum. Meth. Phys. Res. A **403** (1998) 399.

[7] C. Hurtes, M. Boulou, A. Mitonneau and D. Bois, Deep-level spectroscopy in high-resistivity materials, Appl. Phys. Lett. **32** (1978) 821.

[8] S.M. Ryvkin, Photoelectric effects in semiconductors, Consulting Bureau, New York (1965).

[9] R. Vasiliauskas et al, Impact of extended defects on Hall and magnetoresistivity effects in cubic silicon carbide, J. Phys. D: Appl. Phys. **45** (2012) 225102.

[10] G. Lindström et al. Radiation hard silicon detectors - developments by the RD48 (ROSE) collaboration, Nucl. Instrum. Meth. Phys. Res. A **466** (2001) 308–326.

[11] S. I. Parker and C. J. Kenney, Performance of 3-D Architecture Silicon Sensors After Intense Proton Irradiation, IEEE Trans. Nucl. Sci., **48** (2001) 1629-1638.

[12] V. S. Vavilov, N. P. Kekelidze, L. S. Smirnov, Irradiation effects on semiconductors, Moscow, Nauka, 1988.

[13] B. Bogdanovitch, V. Senioukov, A. Koroliov, K. Simonov, Application of low energy electron beams for technology and medicine, Proceedings of the 1999 Particle Accelerator Conference, New York, (1999) 2570.

[14] H. J. Stein. Electrical studies of neutron-irradiated n-type Si: defect structure and annealing, Phys. Rev. **3** (1967) 193.

[15] H.J. Juretschke, R. Landauer, and J.A. Swanson, Hall effect and conductivity in porous media, J. Appl. Phys. **27** (1956) 838.

[16] L.R. Weisberg, Anomalous mobility effects in some semiconductors and insulators, J. Appl. Phys. **5** (1962) 1817-1821.

[17] M. Sze, Physics of semiconductors devices. New York: Wiley, 1981.

[18] J.S.Blakemore, Semiconductor statistics. Pergamon Press. Oxford-London-New York-Paris, 1962.

[19] B. J. Svensson et al. Electronic and dynamical properties of the silicon trivacancy, Phys. Rev. B **86** (2012) 174101.

[20] G. Lindström, , M. Moll, E. Fretwurst. Radiation hardness of silicon detectors – a challenge from high-energy physics, Nucl. Instrum. Meth. Phys. Res. A **426** (1999) 1–15.

[21] J. Dong, D. A. Drabold. Atomistic Structure of Band-Tail States in a-Si. Phys. Rev. Lett. **80** (1998) 1928.

[22] D. V. Lang and L. C. Kimerling. Observation of recombination-enhanced defect reactions in semiconductors. Phys. Rev. Lett. **33** (1974) 489.

[23] M. Bruzzi. Radiation damage in silicon detectors for high-energy physics experiments. IEEE Trans. Nucl. Sci., **48** (2001) 960-971.

Author's published articles:

S1. A. Mekys, V. Rumbauskas, J. Storasta, L. Makarenko, N. Kazuchits, J. V. Vaitkus. Hall and magnetoresistance measurements in fast electron irradiated silicon. Lithuanian Journal of Physics,Vol. 54, No. 2 (2014), 94–99.

S2. A. Mekys, V. Rumbauskas, J. Storasta, V. Rumbauskas, L. Makarenko, J. V. Vaitkus. Defect analysis in fast electron irradiated silicon by Hall and magnetoresistivity means. Nuclear Instruments and Methods in Physics Research B. Vol. 338, 1, (2014), 95–100.

S3. J. V. Vaitkus, V. Rumbauskas, G. Mockevicius, E. Zasinas, A. Mekys, An evidence of strong electron-phonon interaction in the neutron irradiation induced defects in silicon. Nuclear Instruments and Methods in Physics Research A. Vol. 796, (2015), 114-117.

S4. J. V. Vaitkus, A. Mekys, V. Rumbauskas, J. Storasta. Neutron irradiation influence on electron mobility and compensation of dark conductivity in silicon crystals. Accepted in Lith. Journ. Phys. Vol. 56, No. 2 (2016), 67−76.

S5. V. Rumbauskas, D. Meskauskaite, T. Ceponis, E. Gaubas. Anneal induced transforms of radiation defects in heavily electron irradiated Si diodes. Submitted to Journal of INSTrumentation (2016).

Reziumė

Tyrimo problemos, mokslinė svarba, naujumas, mokslinių tyrimų tikslai ir praktinė nauda aptariami įvadiniame skyriuje. Ginamieji teiginiai, ir autorius indėlis taip pat aprašyti įvade. Pirmas skyrius skirtas literatūros apžvalgai. Apžvelgiami radiaciniai defektai silicyje, jų poveikis dalelių detektorių charakteristikoms, taip pat apžvelgiamas radiacinių defektų pasireiškimas galvanomagnetinių reiškinių charakteristikose, motyvuojant šio darbo tyrimus. Antrame skyriuje aptartos tyrimų metodikos ir eksperimentų įranga, taip pat aprašyti ištirti bandiniai. Trečiame skyriuje aptarti tyrimų rezultatai, gauti Holo geometrijos bandiniuose, nagrinėjant Holo efekto ir magnetovaržos charakteristikas, skirtingo laidumo tipo Si medžiagose, apšvitintose 6.6 MeV energijos elektronais, nustatytos sąlygos patikimam krūvininkų sklaidos charakteristikų įvertinimui. Ketvirtame skyriuje aptarti Holo ir foto-jonizacijos spektroskopijos tyrimų rezultatai Holo geometrijos ir diodiniuose Si dariniuose, apšvitintuose reaktoriaus neutronais, dideliais įtėkiais, kuomet galvanomagnetinų reiškinių charakteristikose ir foto-jonizacijos spektruose pasireiškia radiaciniai klasteriai. Penktame skyriuje išnagrinėtos defektų transformacijos 6.6 MeV energijos elektronais apšvitintuose CZ Si dariniuose, juos iškaitinant 80–280ºC temperatūrose. Čia analizuojami DLTS ir mikrobangomis zonduojamo fotolaidumo temperatūrinių kitimų spektroskopijos rezultatai. Pabaigoje apibendrinami tyrimų rezultatai ir pateiktos esminės išvados.

Information about author

Name Surname	Vytautas Rumbauskas
Date of birth, place	14 of September 1985, Joniškis, Lithuania
Address	V. Grybo St. 33-108, Vilnius, Lithuania
Email	vytautas.rumbauskas@ff.vu.lt
Education	2005 Joniškis agricultural school
	2005-2009 Šiauliai University, bachelor course
	2009-2011 Šiauliai University, master course
	2011-2015 PHD student at Vilnius University
Work experience	2012-2015 Engineer (part-time) at Institute of Applied Research, Vilnius University.
	Since 2013 Junior Researcher at Institute of Applied Research, Vilnius University.
Specialization	Investigation of carrier transport, trapping, recombination parameters in semiconductor structures using contact and contactles techniques, radiation defects in semiconductors.